Seismic Radiation From Simple Models of Earthquakes

R. Madariaga

Laboratoire de Géologie de l'École Normale Supérieure,
24 rue Lhomond, F–75231 Paris Cedex 05, France

J.P. Ampuero

Institut fuer Geophysik, ETH Zürich

M. Adda-Bedia

Laboratoire de Geologie of Ecole Noramle Supérieure

We review some basic features of shear wave generation and energy balance for a 2D antiplane rupture. We first study the energy balance for a flat fault, and for a fault that contains a single localized kink. We determine an exact expression for the partition between strain energy flow released from the elastic medium surrounding the fault, radiated energy flow and energy release rate. This balance depends only on the rupture speed and the residual stress intensity factor. When the fault contains a kink, the energy available for fracture is reduced so that the rupture speed is reduced. When rupture speed changes abruptly, the radiated energy flow also changes abruptly. As rupture propagates across the kink, a shear wave is emitted that has a displacement spectral content that decreases like ω^{-2} at high frequencies. We then use spectral elements to model the propagation of an antiplane crack with a slip-weakening friction law. Since the rupture front in this case has a finite length scale, the wave emitted by the kink is smoothed at very high frequencies but its general behavior is similar to that predicted by the simple sharp crack model. A model of a crack that has several kinks and wanders around a mean rupture directions, shows that kinks reduce the rupture speed along the average rupture direction of the fault. Contrary to flat fault models, a fault with kinks produces high frequency waves that are emitted every time the rupture front turns at a kink. Finally, we discuss the applicability of the present results to a 3D rupture model.

1. INTRODUCTION

Dozens of earthquakes have been modeled using kinematic or dynamic methods by the inversion of the seismic waves radiated by these events (see, e.g. Ide and Takeo, 1997, Olsen et al., 1997, Peyrat et al., 2001). Most of these inversions look for flat source models because of either lack of resolution or for lack of knowledge of the geometry of faults. Many authors have recently used geological information and advanced numerical methods to model rupture propagation on complex faults. Among others, three dimensional effects were discussed by Harris and Day (1999)

and Harris et al. (2002) using finite differences,Kame and Yamashita (2003), Aochi and Fukuyama (2002) and Aochi and Madariaga (2003) using boundary integral equations (BIE), and Oglesby et al. (2003) and Duan and Oglesby (2005) using finite elements (FE). In most of these studies the main objective was to understand rupture propagation in complex situations. In a recent study, Aochi and Madariaga (2003) computed the seismic wave field radiated in the vicinity of the Izmit earthquake of 1999. They studied several models of the fault geometry for this event proposed by geologists, seismologists and geodesists. These models differed mainly in the degree of complexity of the fault geometry. They found that geometrical discontinuities have a profound effect on rupture propagation, decreasing rupture speed and generating strong seismic wave radiation. It appears from this study that small scale geometry may play a significant role in energy balance and high frequency radiation by earthquakes.

Recently, in an effort to understand how ruptures interact with fault kinks of arbitrary angles, Polyakov et al. (2002) and Kame et al. (2003) studied in detail the effects of kinks of different angles on the rupture propagation of 2D faults. In a series of experiments Rosakis et al. (1999) and Rousseau and Rosakis (2003) studied ruptures propagating along flat and kinked interfaces at sub Rayleigh and intersonic speeds. What is still lacking in some of these studies is a detailed analysis of seismic wave radiation and energy balance. In a series of recent papers (Adda-Bedia and Arias, 2003, Adda-Bedia, 2004 and Adda-Bedia and Madariaga, 2006) solved the problem of the propagation of an antiplane rupture on a fault with a kink (see Figure 1).

The aim of the present paper is to study a simple 2D model of antiplane rupture and analyze its energy balance and seismic radiation. We first recall some well-established results about seismic energy balance of crack propagation and seismic wave radiation. We show that strong radiation of the ω^{-2} type occurs when rupture changes velocity abruptly, whether a change in rupture speed on flat faults or a change in rupture direction at kinks or other discontinuities. These results are established analytically for a sharp antiplane crack model turning along a single kink but they can be extended to 3D using ray methods (Madariaga, 1977, Bernard and Madariaga, 1984). In particular, we derive the exact energy balance for this model in terms of energy density per unit crack advance, extending the results of Husseini and Randall (1976). We then introduce a numerical model of a fault kink with slip-weakening friction solved by the spectral element method proposed by Komatisch et al. (1998) and Ampuero (2002). We verify that most of the features predicted by the simple crack model appear in the numerical

model, most notably the existence of a kink wave emitted when the rupture front turns at the kink. Finally we model with spectral elements a rupture that propagates along a fault containing a series of kinks with the purpose of simulating a fault that possesses small scale geometrical complexity.

2. RADIATION FROM KINEMATIC AND DYNAMIC RUPTURE MODELS: DISLOCATIONS AND CRACKS

The most frequently used model of seismic radiation from earthquakes is a dislocation of variable amplitude that propagates at more or less constant rupture speed. This model, usually called kinematic, has the advantage of simplicity and provides a simple way to pose the inverse problem of finding the rupture process of an earthquake as a function of time. In general, unfortunately, kinematic models contain a potentially serious problem: unless slip is properly tapered, stresses near the rupture front will be arbitrarily singular and even the continuity of matter may be violated. Let us briefly explain the difficulty: consider a simple dislocation that propagates at constant speed with constant slip. The material on both sides of the fault is homogeneous. We assume that slip as a function of position x and time t is given by

$$D_i(x, y = 0, t) = D_0\,[H(x) - H(x - L)]H(t - X/v_r) \quad (1)$$

where i indicates the in-plane ($i = x$) or anti-plane ($i = z$) component of slip and H denotes the Heaviside step function. This is a constant slip that extends at time t from $x = 0$ to $x = v_r t$. Radiation from this running dislocation model can be fully computed using classical representation theorem techniques (see e.g. chapter 10 of Aki and Richards, 2002). Unfortunately this dislocation model has fundamental flaw:
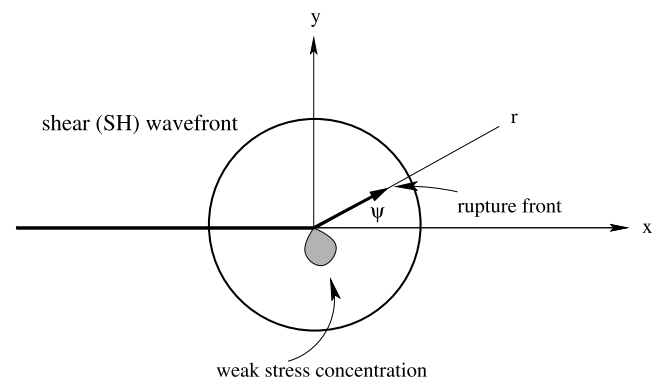

Figure 1. Geometry of the antiplane fault model with a kink. At $x = 0$ the fault changes direction to an angle ψ. We discuss radiation from the kink, and the energy balance of the rupture front.

the amount of energy that flows into the rupture front per unit advance of the dislocation is unbounded. The reason is that slip is discontinuous at the rupture front. This produces interpenetration of matter at the rupture front and is mechanically inadmissible. This of course does not invalidate their use at lower frequencies where energy balance is a secondary consideration.

A better model that avoids interpenetration is to assume that near the rupture front slip is continuous. Very general consideration about energy balance discussed by Kostrov (1964) and Eshelby (1969) among many others show that if slip has a discontinuity of the type

$$D_i(x, y = 0, t) \simeq (v_r t - x)^\lambda H(v_r t - x) \quad (2)$$

behind the rupture front, the energy flow into the crack front is infinite for $\lambda < 1/2$ and zero for $\lambda < 1/2$. Finite energy flow into the rupture front occurs only for the very particular value of $\lambda = 1/2$. This choice fully defines the form of the singularities of stresses and particle velocities near the rupture front, and as a consequence the energy release rate. Actual rupture fronts are of course not truly singular as expected from (2) because the singularity will be distributed by the friction law that controls slip between the two walls of the fault. The approximation (2) is expected to be valid for wavelengths that are longer than the size of the end zone, or cohesive zone, behind the rupture front.

2.1. Rupture Dynamics of a Flat Fault and its Seismic Radiation

Let us recall a few well established results about 2D earthquake dynamics. The radiated field from an antiplane crack moving arbitrarily at subshear speed along a flat fault was solved exactly by Madariaga (1983). Without loss of generality we consider the simpler problem of an antiplane crack running at constant speed v_r along the fault. Ahead of the crack front, located at position $x = v_r t$ at time t, stresses have an inverse square root singularity of the form

$$\sigma_{zy}(x, y = 0, t) = \frac{K_d}{\sqrt{2\pi}} \frac{1}{\sqrt{x - v_r t}} \quad for \quad x > v_r t \quad (3)$$

where K_d is the dynamic stress intensity factor, a quantity with dimensions of stress times the square root of a length that measures the driving stress that makes the crack move. The dynamic stress intensity factor can always be factored into the two terms:

$$K_d = k(v_r) K_* \quad (4)$$

where $k(v_r) = \sqrt{1 - v_r/\beta}$. The second term (K_*) is the residual stress intensity factor, that is the stress intensity that would prevail on the crack tip if the rupture speed v_r were to suddenly drop to zero. In the most of the problems we are going to consider in the following $K_* = K_o$, the static stress intensity factor.

Associated with the singular stress field ahead of the crack front, there is a slip velocity singularity of the same order behind the rupture front:

$$\dot{D}_z(x, y = 0, t) = \frac{2K_d}{\mu\sqrt{2\pi}} \frac{v_r}{\sqrt{1 - v_r^2/\beta^2}} \frac{1}{\sqrt{v_r t - x}} \quad (5)$$
$$for \quad x < v_r t$$

and zero otherwise. Slip has the typical square root behavior behind the crack tip:

$$D_z(x, y = 0, t) = \frac{4K_d}{\mu\sqrt{2\pi}} \frac{1}{\sqrt{1 - v_r^2/\beta^2}} \sqrt{v_r t - x} \quad (6)$$
$$for \quad x < v_r t$$

and is zero outside the crack $(x > v_r t)$.

The full particle velocity field produced by an antiplane rupture front moving at constant speed is very well known, see e.g. chapter 10 of Aki and Richards (2002). For an observer at position (x, y, t) the antiplane particle velocity is given by

$$\dot{u}_z(x, y, t) = \frac{K_d}{\mu\gamma\sqrt{2\pi}} v_r \frac{\left(\sqrt{(x - v_r t)^2 + \gamma^2 y^2} - (x - v_r t)\right)^{1/2}}{\sqrt{2}\sqrt{(x - v_r t)^2 + \gamma^2 y^2}} \quad (7)$$

where $\gamma = \sqrt{1 - v_r^2/\beta^2}$ is the Lorenz contraction factor. This expression can not be used directly to study energy balance because the it does not explicitly identify the point on the fault that emits the radiation that reaches the observer at time t. We can find that point using ray tracing. Let us call retarded time τ the instant of time when the crack emits the wave (7). As follows from Figure 2, at time τ the rupture front is located at $x = v_r \tau$, where τ is the solution of

$$\beta(t - \tau) = \sqrt{(x - v_r \tau)^2 + y^2} \quad (8)$$

We can solve this equation and find

$$\beta(t - \tau) = \frac{v_r}{\beta} \frac{x - v_r t}{\gamma^2} \pm \frac{1}{\gamma^2} \sqrt{(x - v_r t)^2 + \gamma^2 y^2} \quad (9)$$

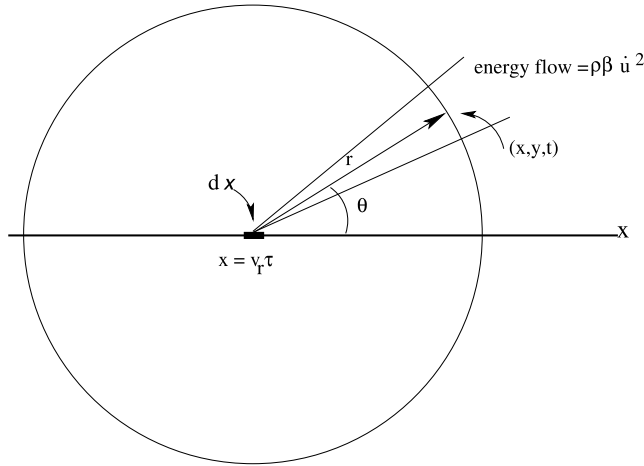Using this expression we can rewrite (7) in the more usual form:

Figure 2. Radiation from a moving antiplane rupture front. The velocity field and the energy flow observed at point (x, y) at time t comes from a well defined fault element. The posiiton of this element can be computed by the retarded time equation (8).

$$\dot{u}_z(x, y, t) = \frac{K_*}{\mu\sqrt{2\pi r}} v_r \frac{\sin(\theta/2)}{(1 - v_r/\beta\cos\theta)}. \qquad (10)$$

Where $r = \sqrt{(x - v_r\tau)^2 + y^2}$ and θ are the cylindrical coordinates drawn around the rupture front as shown in figure 2.

2.2. Energy Balance During Crack Propagation

We can now easily compute the energy radiated by a fault element situated at point $v_r\tau$ on the fault. For this purpose we compute the energy that crosses a circle of arbitrary radius r centered on this point of the fault (see Figure 2).

$$\frac{dE_R(x)}{dx} = e_R(x) = \int_0^{2\pi} \rho\beta\dot{u}^2(r,\theta)\frac{dt}{dx}r\,d\theta$$

Following Adda-Bedia and Madariaga (2006), this integral is independent of the radius r and it can be computed exactly:

$$e_R(x) = \frac{K_*^2}{2\mu}[1 - A(v_r)] \qquad (11)$$

where the factor

$$A(v_r) = \sqrt{\frac{1 - v_r/\beta}{1 + v_r/\beta}} \qquad (12)$$

is the effect of directivity on energy absorption. K_* is the residual stress intensity defined in (4). In (11) we used the

standard convention that energy densities are represented by lower case letters. Let us remark that in computing (11) we did not use any of the classical integral expressions for energy balance due to Kostrov (1964) and others. The radiated energy density e_R was computed here for a crack running at constant rupture speed. It is valid however for arbitrary rupture histories as long as the local rupture velocity v_r is known. (11) shows that radiated energy depends only on the residual stress intensity factor and the instantaneous rupture speed. The history of rupture appears through K_*.

The radiated energy (11) must be compared with the energy absorbed per unit length of crack advance, energy release rate, that is given by:

$$G(v_r) = \frac{K_*^2}{2\mu} A(v_r) \qquad (13)$$

From simple energy balance considerations, the radiated energy per unit crack advance must be the difference between the elastic strain energy released by the body and the energy release rate required to propagate the rupture front by a unit length. There are no other sources nor sinks of energy in this problem. It is well known from Griffith theory in static crack problems that the total energy release per unit crack extension is just the energy release rate for a crack that grows infinitely slowly, i.e. with $v_r \to 0$:

$$e_T = \frac{K_*^2}{2\mu} \qquad (14)$$

which is independent of the current rupture speed. We observe that according to classical fracture mechanics the strain energy release density is just the quasistatic energy release (i.e. as $v_r \to 0$):

$$e_T = G(v_r = 0) \qquad (15)$$

Thus we can write the fundamental energy balance equation

$$e_R(v_r) = e_T - G(v_r) = G(0) - G(v_r) \qquad (16)$$

Using (13) we verify that the radiated energy density is the same as that computed directly from the radiated field (11).

This surprisingly simple expression is exact for our problem where the process zone at the rupture front reduces to a point and there is no healing behind the rupture. Compared to the more general energy balance equation proposed by Kostrov (1974), we have neglected the term due to radia-

tion pressure sometimes called the Kostrov term. Equation (16) was first derived by Husseini and Randall (1976) in an integral form over the entire fault plane. Here we derived it as the local balance of energy flow.

The energy balance equation (16) was determined for the particular case of a semi-infinite crack where the residual rupture speed stress intensity factor K_* was considered a constant. The equation is much more general as long as K_* is computed exactly for more general rupture histories. Several properties of equation (16) are interesting for understanding energy balance in earthquakes. Most authors, like Rivera and Kanamori (2005) write an *energy* balance equation for the entire fault as did Husseini and Randall (1976). Our expression (16) provides a detailed balance of *energy flow* as the rupture front advances with speed v_r. There is no contradiction between the two ways of looking at energy balance, because the residual stress intensity factor K_* contains non-local information about stress drop at other places on the fault. Actually the energy release density e_T knows about stress drop at all already broken parts of the fault.

2.3. High Frequency Radiation From a Rupture Velocity Jump

The energy balance equation (16) is strictly valid for a rupture propagating at a steady rate. It does not yet explain high frequency radiation because if the rupture moves at constant speed it produces a smooth elastodynamic field. In order to apply it to high frequency radiation we have to generalize the expression (10) to rapid changes in rupture speed. We can do this very easily because, as shown initially by Eshelby (1969) and proved later in a more general way by Madariaga (1983), equation (10) completely describes the field radiated by a crack propagating at variable speed. The only change that is required is to interpret $\ell(t) = v_r t$ as the retarded position on the fault of the point that is illuminating the current position (x, y, t) in space and time. This point can easily be found using ray theory.

Let us assume that the rupture speed changes abruptly at position $x = 0$ and time $t = 0$, jumping from a speed v_1 to another speed v_2. Clearly the field radiated before the change in speed is given by (10) replacing $v_r = v_1$. When rupture velocity changes to v_2, the particle velocity field adjust immediately and is now given by the same equation (10), but with $v_r = v_2$. The sudden change in particle velocity field occurs at the wave front $r = \sqrt{x^2 + z^2} = \beta t$ emitted from the point where rupture speed changed abruptly. Across the wave front the particle velocity has an abrupt change in amplitude that is given exactly by

$$\Delta \dot{u}_z(r = \beta t) = \frac{K_o}{\mu \sqrt{2\pi r}} \sin\frac{\theta}{2}\left(\frac{v_1}{1 - v_1/\beta \cos\theta} - \frac{v_2}{1 - v_2/\beta \cos\theta}\right) \quad (17)$$

where r, θ are cylindrical coordinates centered at the origin of coordinates. In the frequency domain, this velocity jump appears as a velocity spectrum decreasing like ω^{-1} or a displacement spectrum decreasing like ω^{-2}. This is the behavior predicted by Brune's model of radiation. The velocity change phases behave just like the stopping phases that are known to produce the ω^{-2} radiation from a circular crack model. Let us remark that there can be no higher order radiation from a dynamic earthquake model. The ω^{-2} behavior in frequency (velocity jump in time domain) is the strongest high frequency phase that can be radiated.

3. RUPTURE FRONT DYNAMICS FOR AN ANTIPLANE FAULT WITH A KINK

The flat fault model provides a simple explanation for the origin of velocity jump pulses that have the typical ω^{-2} decay of the displacement spectrum. For a flat fault such waves can be generated when the crack starts or suddenly stops, or when it abruptly changes rupture velocity as it hits obstacles along the fault. We propose that a simple origin for such obstacles is the geometry of the fault. Fault step-overs, discontinuities and kinks are typical obstacles that may produce strong seismic radiation. In this section we study the effect of a single kink on an antiplane fault. We expect, that with moderate change, the effect of other geometrical features on rupture will be very similar to those of kinks. Rupture propagation across a kink was solved analytically by Adda-Bedia and Arias (2003), and Adda-Bedia (2004). Adda-Bedia and Madariaga (2006) who computed the full elastodynamic field around the crack. Here we discuss the principal results which can be understood without reference to the details of the method used to find the full solution.

Let us consider as in Figure 1 an antiplane fault that has a kink of angle $\psi = \lambda\pi$ at the origin ($x = 0$, $y = 0$). As for the flat fault, the elastic medium surrounding the fault is uniform. Before reaching the kink at time $t = 0$, the fault was running at constant rupture speed v_1. The particle velocity field radiated by the crack before it reaches the kink is given by (7) with $v_r = v_1$. Once the crack reaches the kink, its rupture velocity suddenly changes to v_2 because the stress intensity seen by the kink is less than the stress intensity along the initial fault.

As shown by Adda-Bedia (2004), when the rupture front turns at the kink the dynamic stress intensity factor changes abruptly to

$$K_d(\psi, v_2) \equiv k(v_2)H_{33}(\psi, v_2)\,K_* \quad (18)$$

where K_* is the residual stress intensity of the rupture front before it hits the kink, and $H_{33}(\psi, v_2)$ is a factor that

depends only on the kink angle and the rupture velocity after the kink, v_2. It is quite complex, but it can be computed by the methods proposed by Adda-Bedia and Madariaga (2006). It is convenient to express H_{33} in terms of its static value $H_{33}(\psi, 0)$. This factor is known from the static solution for an antiplane kink (Sih, 1965),

$$H_{33}(\psi, v_2 \to 0) = \left(\frac{\pi - \psi}{\pi + \psi} \right)^{\frac{\psi}{2\pi}}. \qquad (19)$$

In Fig. 3, the function $H_{33}(\psi, v_r/\beta)/H_{33}(\psi, 0)$ is plotted as a function of the kink angle $\lambda = \psi/\pi$, for several values of the rupture speed v_r. We observe that for low rupture speeds, (19) provides a very good approximation for H_{33}. $H_{33}(\psi, 0)$ is equal to 1 for $\psi = 0$, and it is a decreasing function of ψ. For small kink angles we can approximate $H_{33}(\psi, 0) \simeq 1 - \psi^2/\pi^2$ so that, as could be expected for symmetry reasons, the reduction in stress intensity is quadratic in angle ψ. Thus, at least for relatively low rupture speeds, we expect that the stress intensity factor drops instantly when rupture turns at the kink.

The energy release rate can be computed from the dynamic stress intensity factor (18)

$$G(v_r) = A(v_r) \frac{K_*^2}{2\mu} H_{33}^2(\psi, v_r) \qquad (20)$$

where $A(v_r)$ is the universal function given in (12). This expression should be compared to that of the energy release rate before the kink (13). Thus the energy release rate after the kink depends both on the intrinsic factor H_{33}, which itself depend mildly on rupture speed as shown in Fig. 3, and on the rupture velocity factor $A(v_r)$ which decreases from 1 at $v_r = 0$ to 0 when $v_r \to$
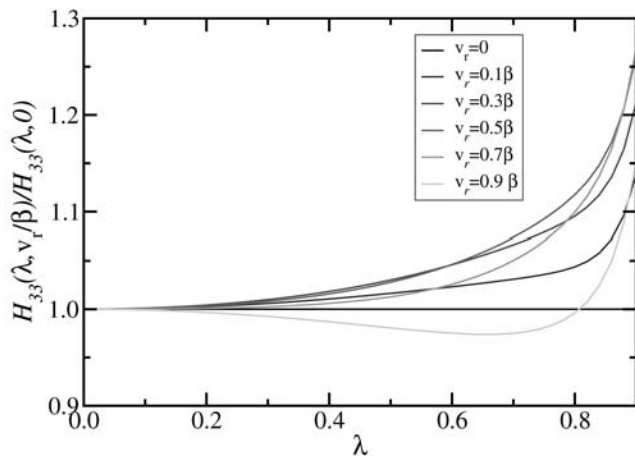

Figure 3. Plot of the function $H_{33}(\lambda, v_r/\beta)/H_{33}(\lambda, 0)$ as a function of the kink angle for some values of the crack tip speed just after the kink. Note that for $\lambda \to 0$, H_{33} reduces to the corresponding elastostatic result given by Eq. (19).

β. It is clear from (18) that when rupture crosses the kink, the energy release rate will in general change abruptly, which will produce a concomitant jump in rupture speed. The only case in which rupture velocity may not change, occurs when the energy absorbed by rupture on both sides of the kink perfectly matches the change in energy release rate (18).

3.1. Seismic Waves Radiated by the Kink

The full particle velocity field radiated by the kink was computed semi-analytically by Adda-Bedia and Madariaga (2006). Just like high frequency radiation from a sudden jump in rupture propagation can be computed as the difference between a starting and a stopping phase, the high frequency waves radiated by the kink can be computed by the difference of two terms: a first term due to radiation from the starting phase of the kink and a second term due to the stopping phase produced by a sudden arrest of the fault. When the crack propagating along the negative x axis with speed v_1 reaches the kink, it emits a strong stopping phase:

$$\dot{u}_z(r, \theta, t) = -\frac{K_*}{\mu\sqrt{2\pi r}} v_1 \frac{\sin(\theta/2)}{1 - (v_1/\beta)\cos\theta} H(t - r/\beta). \quad (21)$$

This stopping phase is immediately followed by a starting phase due to propagation along the kink. This wave has the same wavefront $r = \beta t$ as the previous wave (21) but its amplitude quite complex. Adda-Bedia and Madariaga (2006) showed that the shear wave emitted when the crack starts to move along the kink is:

$$\dot{u}_z(r, \theta, t) = \frac{K_*}{\mu\sqrt{2\pi r}} v_2 R(\theta, \psi, v_2) H(t - r/\beta) \qquad (22)$$

where v_2 is the rupture speed after the rupture front interacts with the kink, $R(\theta, \psi, v_2)$ is a radiation pattern that replaces the $\sin\theta/2$ and the directivity terms in (21) Because the two phases (21) and (22) have different amplitudes, the rupture front has a jump in particle velocity. Its time Fourier transform has the same form as (22), except that $H(t - r/\beta)$ is replaced by $(i\omega)^{-1} exp(-i\omega r/\beta)$. The corresponding displacement has the typical ω^{-2} high frequency behavior. Thus radiation from a kink behaves just like a stopping phase and may explain radiation from earthquakes (Madariaga, 1977).

3.2. Energy Balance at the Kink

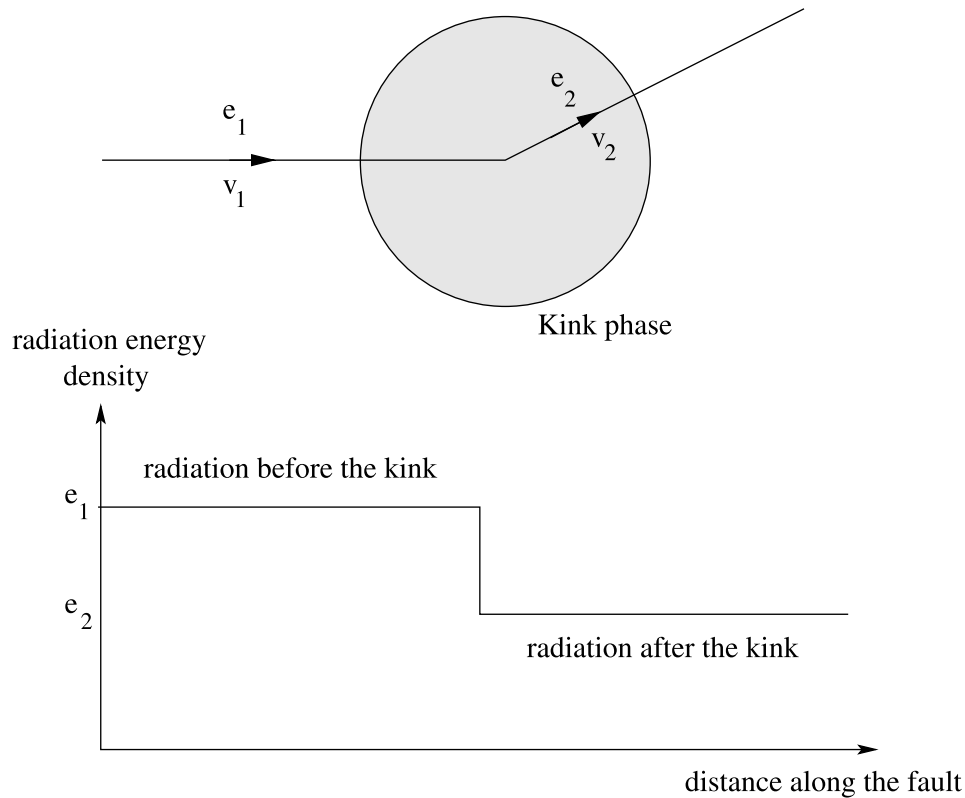The problem of energy balance can be also be solved exactly for the antiplane fault with a kink in the same way as

Figure 4. Variation of radiated energy flow as a function of position along the fault. Before and after the kink the fault generates constant energy fluxes labelled e_1 and e_2, respectively. When rupture turns at the kink it produces a wave front that separates an external region where radiated energy comes from the flat segment of the fault from the stippled region where energy flux comes from the tilted segment of the fault. High frequency radiation occurs because energy flow changes abruptly across the wave front emitted from the kink, this is what we call a kink phase.

it was solved earlier for a flat fault. Before the crack reaches the kink it emits seismic wave energy at a rate given by

$$e_R^1 = (1 - A(v_1)) \frac{K_*^2}{2\mu} \qquad (23)$$

and once it moves into the kink the radiated energy per unit crack advance changes to

$$e_R^2 = [1 - A(v_2)] \frac{K_*^2}{2\mu} H_{33}^2(\psi, v_2) \qquad (24)$$

where H_{33} was defined earlier (18), see Figure 4. It is important to realize that the radiated energy after the rupture has turned at the kink is not determined only by the factor $(1 - A(v_r))$ as in flat cracks, but also by a factor H_{33} that depends on rupture speed and angle. For small rupture speeds we expect that H_{33} becomes independent of rupture speed.

4. NUMERICAL MODELING OF FAULT KINKS

In the previous sections we established a detailed energy balance equation for a sharp crack running at variable speed along a fault that contains a kink. We also examined the waves radiated by the kink We will now examine the properties of a kink on a fault where rupture is controlled by a friction law that contains a finite process zone. Let us consider for that purpose the kink shown in Figure 1. Seismic wave propagation with frictional boundary conditions was modeled using the spectral element method proposed by Komatisch and Vilotte (1998) with the split-node crack boundary conditions developed by Ampuero (2002), following Andrews (1999). Details of the numerical technique can be found in those publications, the particular program we used is publicly available in Ampuero's (2005) web site. For the numerical computation we divide the rectangular elastic medium into a mesh of structured quadrangular elements as shown in Figure 5. The elastic displacement field inside each quadrangular element was
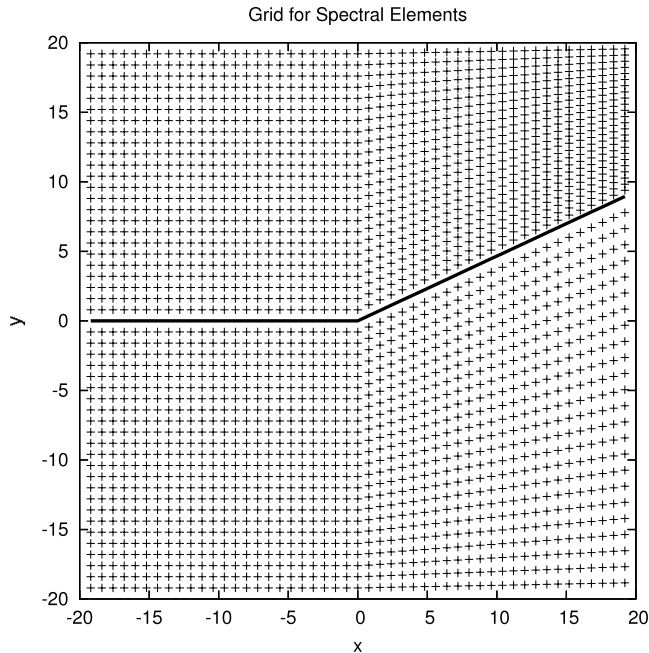
Figure 5. The spectral element grid used to model rupture propagation along a fault containing a kink at the origin. The fault is figured by the thick continuous line. Rupture propagates spontaneously under the control of a slip weakening friction law.

interpolated by a degree 7 Lagrange polynomial and integration was computed at 8x8 Gauss-Lobato points inside each element. The elastic medium was assumed to be uniform with elastic properties (ρ = 2670 kg/m^3, β = 3464 km/s). The fault contains a kink of angle ψ. We chose 20 degrees for the particular example of Figure 5. The total size of the grid is 20x20 km, with a grid spacing of 800 m in the horizontal direction and variable spacing in the vertical one. The maximum distance between Gauss-Lobato points was 276.2 m and the minimum was 35.79 m. The spectral element equations were solved by a predictor corrector time marching scheme based on the Newmark's method. In our simulations we used α = 1, β = 1/2 and γ = 1 as suggested by Festa and Vilotte (personal communication, 2006). The time step was chosen so that the maximum value of the CFL parameter for the simulation was exactly 0.5. For the particular case of the mesh shown in Fig. 5 the time step was Δt = 0.005167 s.

The boundary conditions on the fault are as follows. Before the rupture starts we assume that a uniform antiplane stress field σ_{yz} = 70 MPa acts on the entire elastic medium. This is the initial stress on the flat part of the fault; along the kink the initial shear stress is $\sigma_{yt}^0 = \sigma_{yt} * \cos\psi = 65.52$ MPa. On the fault we apply a uniform slip weakening friction law:

$$\sigma_{yt} = T_d + (T_u - T_d)\frac{D}{D_c} \qquad for \qquad D < D_c \qquad (25)$$

$$= T_d \qquad\qquad for \qquad D > D_c \qquad (26)$$

once the fault begins to slip. Since antiplane faults do not produce changes in normal stress there is no coupling between normal and tangential stresses. In the computations shown here we assumed T_u = 80 MPa, T_d = 63 MPa, D_c = 0.5 m. Thus, complete stress drop on the horizontal segment of the fault is $\Delta\sigma = 7$ MPa and 2.52 MPa on the kinked segment. In order to start rupture we introduce a small zone of the fault where the initial stress σ_{yt}^0 was increased to 88 MPa, that is larger than T_u. These numerical values were taken from the SCEC blind test for earthquake dynamics codes (Harris and Archuleta, 2004).

4.1. Results of Numerical Modeling for a Single Kink

In Plate 1 we show the elastodynamic field around the fault produced by the propagation of rupture. Each row in this Figure shows particle velocities and stresses at regular intervals in time. The columns show, from the left, particle velocities and the two relevant components of stress. Before the rupture hits the kink the elastodynamic field shows all the usual features expected for antiplane cracks. Stress σ_{zy} is the shear stress acting on the fault. It drops from its initial value to the kinematic friction level on a broad zone around the fault. Particle velocity on the first row is clearly divided into an upper positive zone $\dot{u}_z$ above the fault and a negative one below it. Velocity and shear stress concentrations are clearly visible near the rupture front. Finally shear stress on vertical planes, σ_{zx} shows a typical quadrantal distribution centered on the initial asperity.

Once the rupture hits the corner of the kink, the velocity and stress fields change substantially. The most important feature is the cylindrical (we are in 2D) wave front that propagates away from the corner at the shear wave speed. This wave front is clearly observed in both particle velocities and stress components as predicted by our analytical approximation of a sharp crack without slip weakening. Thus in spite of the smoothing produced by the slip weakening friction law we observe a clear shear wave. Near the rupture front along the kink, we observe the white spots that represent the strong velocity and stress concentrations that drive the fault along this segment. We conclude that a numerical model of the kink produces results that are in broad qualitative agreement with the sharp shear crack model studied by Adda-Bedia and Madariaga (2006). Direct comparison between numerical and analytical models is not possible because we can not model a sharp crack numerically.
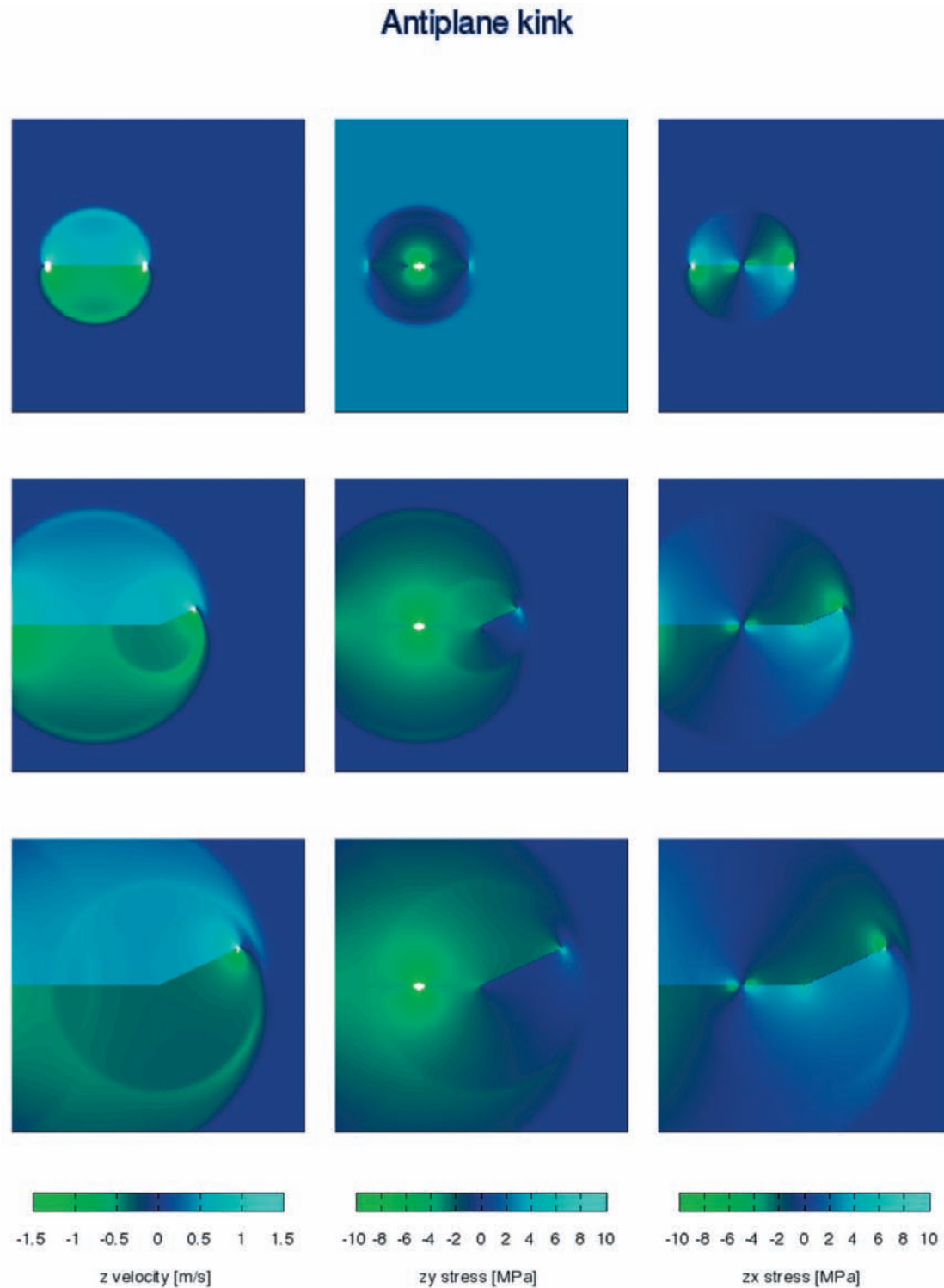
Antiplane kink

Plate 1. Numerical simulation of rupture propagation along the fault shown in Figure 5. The Figure shows velocity $\dot{u}_z$ (left) and the stress fields σ_{zy} and σ_{zx} (middle and right) at three successive instants of time. On the top line the elasto-dynamic fields at the instant when rupture reaches the kink. The following rows show the fields at two instants of time after the rupture propagated beyond the kink.

5. A FAULT MODEL WITH A GEOMETRICALLY COMPLEX FAULT

The initial motivation for the present work was the observation by Aochi and Madariaga (2003) that a simple modification of the fault geometry of the Izmit earthquake could produce vastly different ruptures. If the fault was modeled with a single smooth fault surface, rupture propagated very rapidly along the fault reaching super-shear speeds. Adding a small amount of geometrical discontinuities (kinks) to the fault, as suggested by many geological and geodetic studies of the Izmit earthquake, reduced rupture speed substantially, but the most curious phenomenon we observed was that kinks generated seismic waves that looked like seismic noise. The Izmit model studied by Aochi and Madariaga (2003) was a 3D fault solved using a combination of boundary integral equations for modeling the rupture process and finite differences for the computation of the wave field around the fault. In this section we study a less ambitious model, an antiplane fault with the geometry shown in Fig. 6. The fault is flat from a long wavelength perspective, but it is geometrically complex at the smaller scale. We envision this model as a generic model for more geometrical complexities in faults.

In Fig. 6 we show the geometry of the fault embedded in a uniform isotropic elastic medium that we study numerically by the spectral element method. The rectangular box is 30 by 20 km long and the grid used to simulate wave propagation with spectral elements is highly structured with equal griding of 800 m in the horizontal direction and variable grid spacing in the vertical one. All elements are quadangular and, contrary to most automatic mesh generators all corners of the grid have exactly four neighboring elements. This is essential for accurate modeling of the fault dynamics. All other parameters are the same as for the single kink. As before, a uniform initial shear stress field $\sigma_{zy} = 70$ MPa was assumed. The initial shear stress on every segment of the fault was computed by projection of this stress field using $\sigma_{zt} = \sigma_{zy} \cos \psi_i$, where ψ_i is the angle with respect to the horizontal of each of the fault segments.

Plate 2 shows the field radiated by the complex fault at three equally spaced instants of time. Each row represents an instant of time and the columns are, particle velocity ($\dot{u}_z$) and stresses (σ_{zy} and σ_{zx}). The kink phases emitted from the fault each time that the rupture front turns at a kink are clearly observed in all three field components. Although these kink phases are smoothed by the slip weakening friction law with respect to those computed earlier for the sharp fault, they still are characterized by a sharp change in particle velocity and shear stresses. Such waves behave at high frequencies as step functions in velocity and, therefore, as ω^{-2} in displacement spectra. Thus as the rupture advances it intermittently emits kink phases that contribute to seismic radiation at high fre-
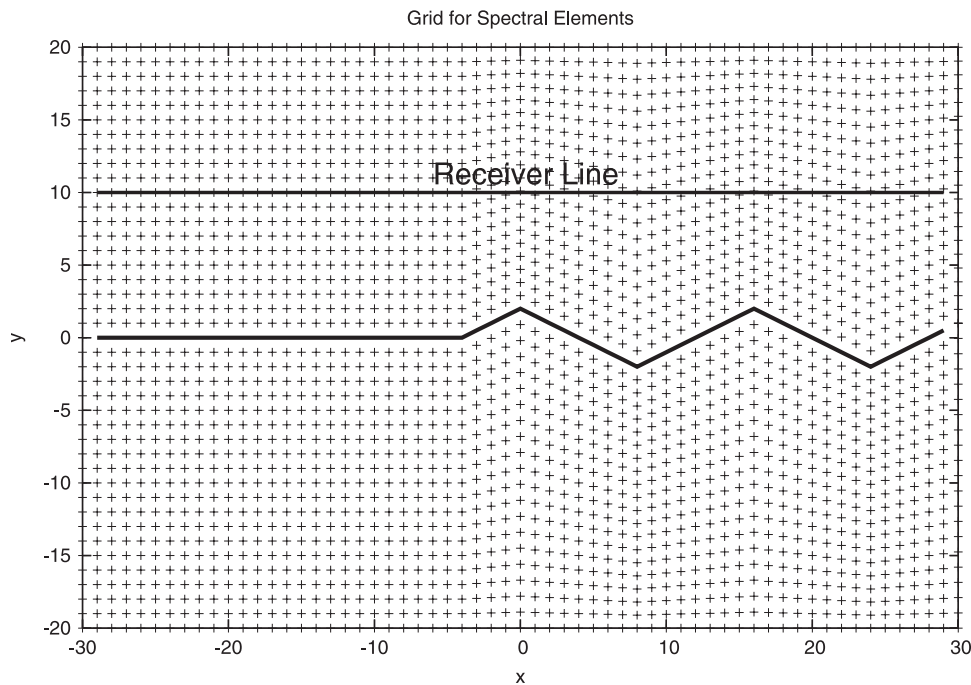

Figure 6. The spectral element grid used to model antiplane rupture propagation along a fault containing several kinks. The fault is figured by the thick continuous line. The seismograms shown in Figure 7 were computed along the receiver line.
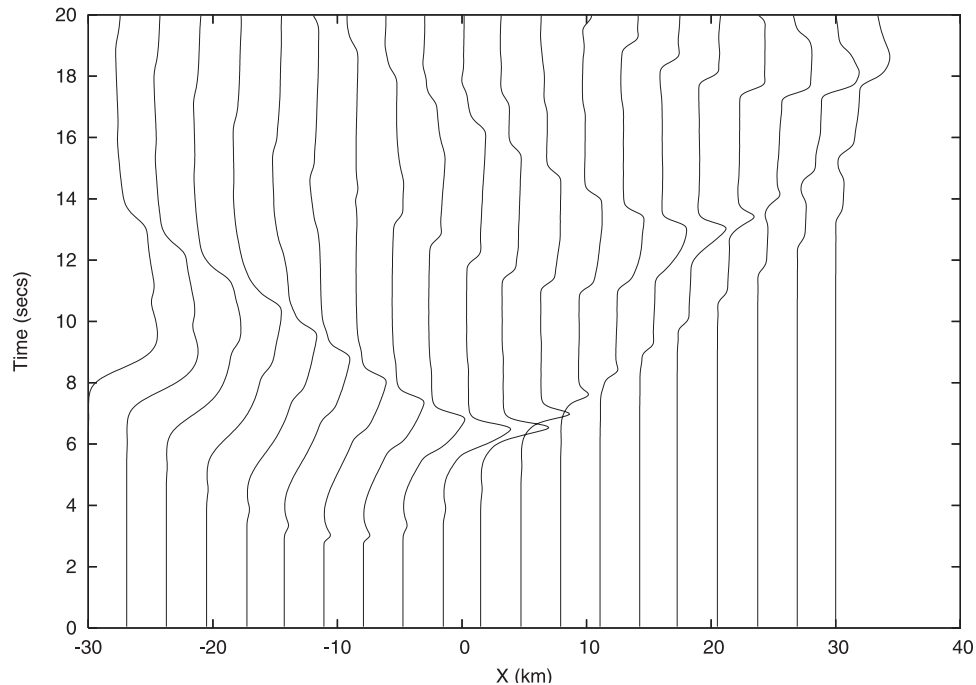
Figure 7. Seismograms computed along the receiver line shown in Figure 6. These seismograms show particle velocity as a function of position along the receiver line and time. We observe multiple kink phases emitted from each of the corners of the fault of Figure 6.

quencies. This is clear in the synthetic seismograms plotted in Figure 7. These seismograms were computed along a line parallel to the average strike of the fault, situated 10 km away from it as shown in Figure 6. The seismograms are dominated by the kink phases emitted by the propagation of the rupture front along the complex fault. Each of these phases has the velocity jump predicted from the simple kink model of previous section. The jumps are smoothed by the finite slip-weakening distance of the friction law used in the simulation.

Another important feature of this model is that the kinks along the fault produce a significant drop in apparent rupture speed. In plate 3 we plot slip and shear stress on the fault as a function of horizontal distance along the centerline of the fault. The rupture front slowness observed in both figures increases rapidly once the rupture front enters the zone with kinks. This increase in slowness, means that the apparent rupture speed in the direction of the axis x has decreased due to energy loss due to the combined effect of a decrease in stress concentration that occurs when the crack turns at the kink, but also by the energy radiated by kink waves. The reduction in true speed, the rupture front speed along each segment of the fault, is even more pronounced. Thus, as noticed by Aochi and Madariaga (2003) in their simulations of the Izmit earthquake, the combined effect of geometrical discontinuities is to reduce rupture speed and produced enhanced seismic radiation.

6. DISCUSSION AND CONCLUSIONS

We have established a detailed energy balance equation for an antiplane crack containing either barriers or geometrical obstacles like a simple kink. The results can be extended to more complex faults containing large numbers of kinks, barriers and other geometrical discontinuities. In this simple 2D model the ratio of radiated energy to energy release rate is entirely determined by the local rupture velocity and the residual stress concentration K_*. This may appear as an apparent violation of Rivera and Kanamori (2005), but it is not because K_* contains information about strain energy release in the rest of the elastic body. We emphasize again that our statements concern energy flow not total radiated energy.

The energy balance equation (16) can be extended to flat faults in mode II for ruptures running at sub-Rayleigh speeds. The expressions for the effects of rupture velocity are slightly more involved than in the present case, because $A(v_r)$ (see, e.g. Freund, 1990 chapter 5) is very complex. For mode II cracks running at supershear speeds we expect that the energy balance will be very complex and needs to be investigated. For kinks in mode II there is no theoretical results similar to those of Adda Bedia and Madariaga (2006). We expect however that a running mode II fault hitting a kink will produce mixed mode ruptures
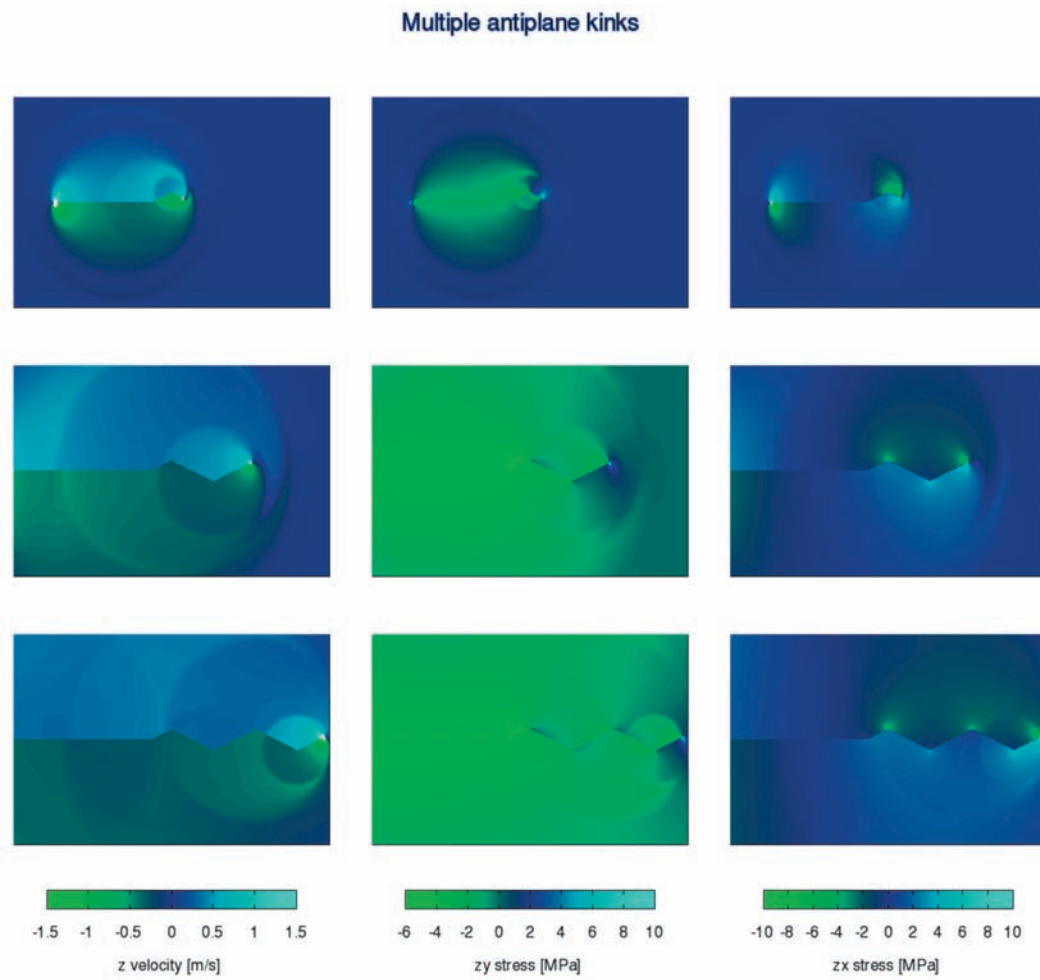
Plate 2. Numerical simulation of rupture propagation along the fault shown in Figure 6. The Figure shows velocity $\dot{u}_z$ (right) and the stress fields σ_{zy} and σ_{zy} (middle and left) at three successive instants of time.
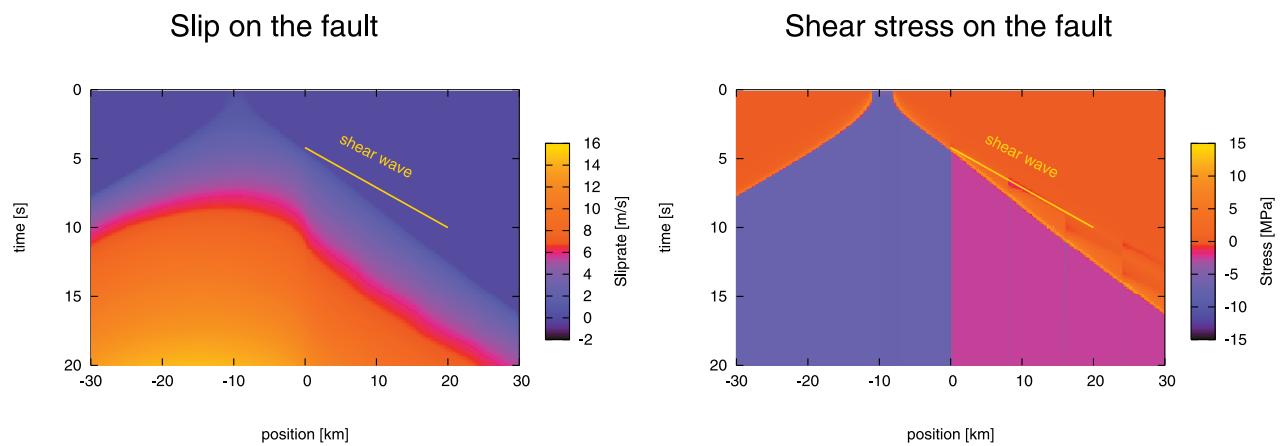

Plate 3. Numerical simulation of rupture propagation along the fault shown in Figure 6. The Figure on the top shows slip as a function of position along the fault and time. The bottom pircture shows the corresponding stress field. The short yellow line shows the slope of a wave propagating at the shear wave speed. Rupture speed reduces significantly once the fault propagates beyond the beginning of zone of complex geometry.

unless the confining stresses are large enough as shown by preliminary results by Festa and Vilotte (personal communication, 2006).

For 3D problems the equation of energy flow balance (16) still applies locally as long as the curvature of the rupture front is small. From simple geometrical arguments presented by Madariaga (1977) we expect that a local energy balance equation can be established in 3D for a rupture front that stops, or changes speed, synchronously in its entire length. In that case the velocity field (10) will be multiplied by a factor

$$\sqrt{\frac{R_\kappa}{R + R_\kappa}} \tag{27}$$

where R is the distance to the rupture front and R_κ is the radius of curvature of the rupture front. For small distances, less that R_κ, the factor tends to 1 and we have basically a 2D problem. For large R, on the other hand, the factor tends to $\sqrt{R_\kappa/R}$, so that geometrical spreading in (10) will become of order R^{-1} as expected for three dimensional sources. For more general rupture problems where the rupture front has a different curvature from the barrier, it is still possible to get simple expressions for radiation using the isochrone method of Bernard and Madariaga (1984). It is very likely, however, that in three dimensional problems, the assumption that friction remains constant behind the rupture front is no longer valid. Healing, either spontaneous or due to the effect of lateral boundaries of the fault will reduce the available strain energy.

We showed that for 2D faulting, high frequency radiation is intimately connected to detailed energy balance, the way energy is partitioned near the rupture front as it propagates along preexisting faults. We found that for an antiplane fault the high frequency waves are emitted by changes in rupture speed. Either changes in speed for flat faults, or changes in the direction of rupture propagation for faults that contain kinks and other discontinuities. When faults contain kinks, energy balance and rupture velocity adjusts instantaneously as the rupture crosses the cusp of the kink. At the same time cylindrical shear wave is emitted. This wave front produces a jump in particle velocity, with a concomitant change in radial stresses. Such waves have a spectral decay of ω^{-1} in particle velocity, or ω^{-2} in displacement. The agreement with observed spectra of many earthquakes is interesting. This is then a potential candidate for the origin of high frequency seismic waves radiated by earthquakes. Even if it is not possible at present to establish full 3D energy balance equations, it is very likely that kinks in 3D will also produce ω^{-2}-like radiation. This is because the rupture front will very likely interact with kinks such that the apparent rupture speed of the crack will very often be supersonic along the edge of the kink producing again ω^{-2} waves as discussed by Bernard and Madariaga (1984). Numerical modeling in 3D is currently in progress in order to better understand energy balance in 3D.

We also modeled numerically a fault containing a series of geometrical discontinuities (kinks). The main effect of the kinks is to slow down rupture significantly. Although we still have to do more general models of fault complexity and analyze them statistically, our results indicate that apparent rupture speed for complex faults must be carefully interpreted. In particular, estimates of energy release rate made from flat fault models and constant rupture speed, may be contaminated by the effects of energy lost as radiated waves. Our results also show that as ruptures propagate crossing kinks and other geometrical discontinuities, they emit high frequency waves that may be very difficult to model with deterministic models.

REFERENCES

Adda-Bedia, M. and R. Arias, Brittle fracture dynamics with arbitrary paths–I. Dynamic crack kinking under general antiplane loading, J. Mech. Phys. Solids, 51, 1287–1304, 2003.

Adda–Bedia, M. and R. Madariaga, Seismic radiation from a kink on an antiplane fault, submitted to *Bull. Seismol. Soc. Am.*, 2006.

Adda–Bedia, M., Brittle fracture dynamics with arbitrary paths–II. Dynamic crack branching under general antiplane loading, J. Mech. Phys. Solids 52, 1407–1420, 2004.

Aki, K. and P. G. Richards, Quantitative seismology, 2nd Ed. University Science books, Sauzalito, Ca, 2002.

Ampuero, J. P., SEM2DPACK, A Spectral Element Method tool for 2D wave propagation and earthquake source dynamics available at http://www.sg.geophys.ethz.ch/geodynamics/ampuero, 2005.

Ampuero, J.–P. Etude physique et numérique de la nucléation des séismes. Ph. D. thesis, Université Paris 7, Denis Diderot, Paris, 2002.

Andrews, D. Test of two methods for faulting in finite difference calculations. Bull. Seis. Soc. Am. 89, 931–937, 1999.

Aochi, H. and E. Fukuyama, Three dimensional non–planar simulations of the Landers earthquake, J. Geophys. Res., 107, 2035, doi:10.129/2001JB000061, 2002.

Aochi, H., E. Fukuyama and R. Madariaga, Constraint of fault parameters inferred from nonplanar fault modeling, Geochem. Geophys. Geosys., 10.1029/2001GC000207, 2003.

Aochi, H. and R. Madariaga, The 1999 Izmit, Turkey, earthquake: non–planar fault structure, dynamic rupture process, and strong ground motion, Bull. Seismol. Soc. Am., 93, 1249–1266, 2003.

Bernard, P. and R. Madariaga, High frequency seismic radiation from a buried circular fault. *Geophys. J.R. Astr. Soc.*, , 1–18, 1984.

Duan, B. and D. D. Oglesby, Multicylce dynamics of a non–planar strike slip fault. J. Geophys. Res., 110, B03304, doi:10.1029/2004JB003298, 2005.

Eshelby, J. D., The elastic field of a crack extending nonuniformly under general antiplane loading, J. Mech. Phys. Solids 17, 177–199, 1969.

Freund, L. B., 1990. Dynamic Fracture Mechanics. Cambridge University Press, New York.

Harris, R. A., and R. J. Archuleta, Seismology: earthquake rupture dynamics: comparing the numerical computation methods, EOS Trans. AGU, 85(34), 321, 2004.

Harris, R. A. and S. Day, Dynamic 3D simulations of earthquakes on an echelon faults, Geophys. Res. Lett., 26, 2089–2092, 1999.

Harris, R. A., J. F. Dolan, R. Hartleb and S. M. Day, The 1999 Izmit, Turkey, earthquake: A 3D dynamic stress transfer model of intra–earthquake triggering, *Bull. Seismol. Soc. Am.*, **92**, 245–255, 2002.

Husseini, M. I. and M. J. Randall, Rupture velocity and radiation efficiency, Bull. Seismol. Soc. Am., 66, 1173–1187, 1976.

Ide, S. and M. Takeo, Determination of constitutive relations of fault slip based on seismic wave analysis, J. Geophys. Res., 102, 27239–27391, 1997.

Kame, N., J. R. Rice and R. Dmowska, Effects of prestress state and rupture velocity on dynamic fault branching, J. Geophys. Res., 108, 2265, doi:10.1029/2002JGB002189, 2003.

Kame, N. and T. Yamashita. Dynamic branching, arresting of rupture and the seismic wave radiation in self-chosen crack path modeling, Geophys. J. Int., 155, 1042–1050, 2003.

Komatitsch, D. and J. P. Vilotte . The spectral element method: an efficient tool to simulate the seismic response of 2D and 3D geological structures. Bull. Seis. Soc. Am. 88, 368–392, 1998.

Kostrov, B. V., Seismic moment and energy of earthquakes and seismic flow of rocks, Izvestia: Earth physics, 1, 23–40, 1974.

Madariaga, R., High-frequency radiation from dynamic earthquake fault models, Ann. Geophys., 1, 17–23, 1983.

Madariaga, R., High-frequency radiation from crack (stress drop) models of earthquake faulting, Geophys. J. Roy. Astr. Soc., 51, 625–651, 1977.

Oglesby, D. D., S. M. Day, Y-G Li and J. E. Vidale, The 1999 Hector Mine earthquake: the dynamics of a branched fault system, Bull. Seismol. Soc. Am., 93, 2459–2476, 2003.

Olsen, K. B., R. Madariaga and R.J. Archuleta, Three-dimensional dynamic simulation of the 1992 Landers earthquake, Science, 278, 834–838, 1997.

Peyrat, S., K. B. Olsen, and R. Madariaga, Dynamic inversion of the Landers earthquake, J. Geophys. Res. 2001.

Polyakov, A., R. Dmowska and J. R. Rice, Dynamic shear rupture interactions with fault bends and off-axis secondary faulting, J. Geophys. Res., 107, 2295, doi:10.1029/2001JB000572, 2002.

Rivera, L and H. Kanamori, Representations of the radiated energy in earthquakes, Geophys. J. Int., 162, 48–155, 2005.

Rosakis, A. J., O. Samudrala and D. Coker, Cracks faster than the shear wave speed, Science, 284, 1337–1340, 1999.

Rousseau, C. E. and A. J. Rosakis, On the influence of fault bends on the growth of sub-Rayleigh and intersonic dynamic shear ruptures, J. Geophys. Res., 108, 2401–2431, doi:10.1029/2002JGB002310, 2003.

Sih, G. C., Stress distribution near internal crack tips for longitudinal shear problems, J. Appl. Mech., 32, 51–58, 1965.